Journal of Materials Chemistry A

ROYAL SOCIETY OF CHEMISTRY

PAPER

View Article Online
View Journal | View Issue

Check for updates

Cite this: *J. Mater. Chem. A*, 2022, **10**, 25319

Mn(II)-doped CdS/ZnS core/shell quantum dot films photocatalyze reductive organic transformations with a boost in efficiency from enhanced Auger processes†

Brian Malile,[a] Rana Sodhi [b] and Jennifer I. L. Chen *[a]

Received 24th August 2022
Accepted 5th November 2022

DOI: 10.1039/d2ta06727g

rsc.li/materials-a

We investigated the reduction of organic compounds photocatalyzed by Mn^{2+}-doped CdS/ZnS quantum dot (Mn:CdS/ZnS QD) films. The incorporation of Mn^{2+} ions into CdS nanocrystals as a dopant promotes Auger cross-relaxation, a phenomenon that yields hot electrons with high reducing power. Using QD-coated vessels or substrates, we examined several model organic reactions to establish the versatility and superior performance of Mn:CdS/ZnS QDs over undoped CdS QDs. First, Mn:CdS/ZnS QDs exhibited a 3.4-fold increase in the photoreduction of methyl viologen compared with CdS QDs. Second, the viologen can subsequently be utilized as an electron shuttle in biphasic reactions, such as the photoreduction of *meso*-stilbene dibromide, allowing for flexible design where reactants were separate from the photocatalysts. Third, Mn:CdS/ZnS QDs photocatalyzed the 6-electron reduction of nitrobenzene to aniline with an overall internal quantum efficiency of ~3%. Impressively, the photoreduction of nitrobenzene was complete in 15 min by doped QDs *vs.* >48 h by undoped QDs – an enhancement of >190-fold. Moreover, we investigated the recyclability of the Mn:CdS/ZnS film and detected changes in the surface species, indicating some oxidation of the film upon its use as a photocatalyst. Different from previous studies, the QD films and coatings facilitate the rapid separation of catalysts from solution and significantly reduce post-reaction workups. Our work demonstrates a drastic improvement in the efficiency of CdS QD-based photocatalysis that may have broad implications in photoredox reactions.

Introduction

Semiconducting nanocrystals with sizes smaller than the exciton Bohr radius, known as quantum dots (QDs), are emerging catalysts for photoredox reactions.[1] These reactions are traditionally performed using expensive iridium and ruthenium complexes. Contrary to molecular catalysts, QDs exhibit desirable properties such as tunable reduction and oxidation potentials, long-lived excited states, and broad absorption spectra,[2–4] which can be achieved by controlling the size and surface chemistry. Importantly, an individual QD can provide numerous reaction sites and facilitate multielectron reduction processes,[5] and QD catalyst loadings down to 0.0001 mol% have yielded promising turnover numbers.[6] Previous studies on photocatalysis with QDs have mainly focused on CdS for hydrogen production,[7] small molecule activation,[8] C–C bond coupling,[9] and functional group reduction.[10] On the other hand, challenges for retaining stable and efficient QDs for photocatalytic reactions remain; there is a need to optimize sacrificial agents, shorten reaction times, and reduce surface recombination of charge carriers.[11] Besides size control, the introduction of dopants into QDs can lead to new or enhanced photophysical properties. For example, Mn^{2+}-doping in QDs leads to enhanced Auger processes that generate hot electrons with increased reductive power.

Auger cross-relaxation is a nonradiative event where the energy from the annihilation of an exciton transfers to a second electron in the conduction band (CB), making it a hot electron.[12] The probability of this process is enhanced in QDs compared with the bulk material because quantum confinement promotes the interaction between charge carriers and conservation rules on momentum are relaxed such that only energy needs to be conserved.[12,13] Auger cross-relaxation is further enhanced in Mn-doped QDs because the Mn^{2+} ion serves as an intermediate, highly localized energy storage site. Mn^{2+} has a long-lived excited state (~millisecond for $^4T_1$, the lowest excited state in a tetrahedral weak ligand field) that increases the probability of

[a]*Department of Chemistry, York University, 4700 Keele Street, Toronto, M3J 1P3, Ontario, Canada. E-mail: jilchen@yorku.ca*

[b]*Ontario Centre for the Characterization of Advanced Materials, Toronto, M5S 3E4, Ontario, Canada*

† Electronic supplementary information (ESI) available: Experimental details, energy level diagram, and additional NMR and PL data. See DOI: https://doi.org/10.1039/d2ta06727g

Auger-type energy transfer from Mn* to a conduction band electron.[14,15] Notably, in Mn-doped QDs, hot electrons having ~2.1 eV excess energy can be generated under light intensity comparable to solar irradiation, where the exciton-to-Mn energy transfer from the first photon absorption can be given to an electron created by a second photon absorption. The spin-exchange interactions between the magnetic dopant (Mn^{2+}) and host material (CdS) dramatically enhance the Auger process such that the Mn^{2+}-assisted energy transfer to conduction band electrons outcompetes the intraband cooling, in turn increasing the number of hot carriers.[16,17] The properties of the hot electrons were investigated photoelectrochemically and in solid-state device studies. Injected electrons quenched the Mn^{2+} photoluminescence and the resultant hot electrons crossed blocking layers having empty states higher in energy than the conduction band of the QD semiconductor.[14,15,18] The hot electrons from Mn-doped QDs are much higher in energy than those from plasmonic nanoparticles, even approaching the vacuum level.[17,19] Therefore, harnessing hot electrons from Mn-doped QDs may facilitate reactions previously unfeasible under mild conditions. On the other hand, the use of hot electrons from Mn-doped QDs for chemical transformation has focused on solar-related applications[20] such as water splitting[21,22] and CO_2 reduction.[23] It has been found that Mn-doped QDs exhibited up to 7-fold enhancements compared with undoped dots for H_2 production,[24] and that electron transfer from Mn-doped QDs can occur over a long range yielding different selectivities and product yields.[25] Motivated by an increasing interest in developing QDs as efficient heterogeneous catalysts, we set out to investigate Mn-doped QDs as photocatalysts for organic transformations, which has not been reported to date.

Herein, we investigated Mn^{2+}-doped CdS/ZnS core/shell QDs (denoted as Mn:CdS/ZnS or doped QDs) as photoredox catalysts for model organic reactions. We examined three reactions and compared the performance of doped QDs with that of the undoped (CdS) QDs: (1) photoreduction of methyl viologen; (2) dehalogenation of *meso*-1,2-dibromo-1,2-diphenylethane; and (3) photoreduction of nitrobenzene to aniline. Different from existing studies on QD-catalyzed organic transformations, we implemented the QDs as films and coatings directly on the reaction vessels. The film setup permits the facile removal and recycling of the QD photocatalysts from the reaction mixture and their use in various types of solvents. In addition to demonstrating the superior photocatalytic capabilities of Mn:CdS/ZnS QDs, we show that the film setup enables efficient post-reaction workup without laborious purification to separate the catalysts, thereby overcoming the drawback of colloidal-based suspensions. Our work opens the door for a wider exploration of Mn-doped QDs for use in synthetic and process chemistry where catalyst-coated reaction vessels may be of interest.

Results and discussion

Supported Mn-doped CdS/ZnS QD films as photocatalysts

Scheme 1 illustrates the QD-coated system (left), the photophysical processes that generate the hot electrons upon light excitation (centre), and the reactions examined (right). Blue light irradiation creates an exciton, the energy of which rapidly transfers to the Mn^{2+} ion resulting in a $^4T_1$ excited state.[26] Because of the long-lived excited Mn^{2+} state, non-radiative Auger cross-relaxation occurs with a high probability when additional conduction electrons are present, leading to hot electron generation.[14] The cross-linked QDs in a film further promote the Auger process due to the interparticle shuttling of the excited electrons prior to radiative relaxation.[27] The photogenerated electrons were exploited for three model reactions (Scheme 1, right) to elucidate the reducing capabilities of the doped *vs.* undoped QDs.

To study heterogeneous photocatalytic reactions, we incorporated Mn:CdS/ZnS core/shell QDs as films on glass to simplify the post-reaction recovery of photocatalysts by eliminating the need to separate the QDs *via* multiple rounds of centrifugation. The Mn:CdS/ZnS QDs were synthesized by a previously established hot-injection method[14] and subsequently capped with 2-monolayers of a ZnS shell and terminated with a Zn^{2+} layer. The undoped CdS/ZnS QDs were synthesized similarly without the Mn precursor. We installed a thin ZnS shell to passivate surface trap states[28] while allowing carriers to tunnel through. Without the ZnS shell, the energy transfer to the Mn^{2+} ion in the doped QDs was impeded by the nonradiative recombination pathways of the trap states. Fig. S1† shows the PL spectra of the as-synthesized doped and undoped CdS core QDs with an increasing number of monolayers of the ZnS shell. The increase

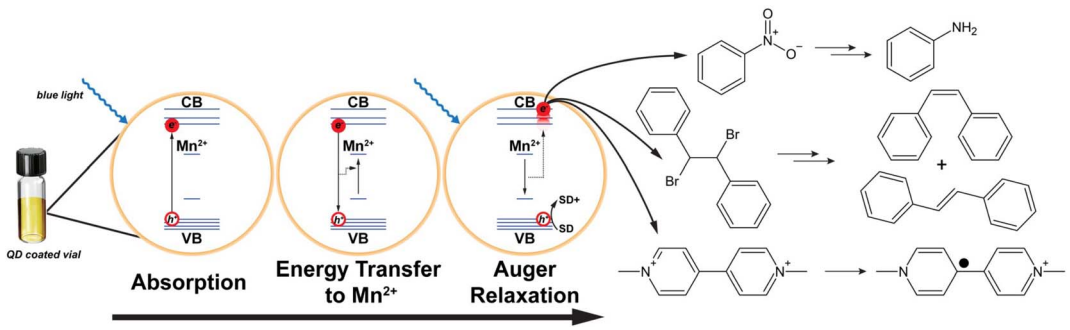

Scheme 1 Mn^{2+}-assisted Auger relaxation generates hot electrons that are to be harvested for photoreduction reactions. The electron and hole transfer to the organic substrate and sacrificial donor (SD), respectively.

in PL of the QDs with an increasing number of ZnS layers suggests successful passivation.

The purified QDs were immobilized on glass vessels (*e.g.*, slides or vials) *via* evaporation-assisted deposition and then cross-linked with heptanediamine to yield mechanically stable films. The molar ratio of Mn to Cd was determined to be 0.0171 ± 0.0002 : 1 by inductively coupled plasma optical emission spectroscopy (ICP-OES, see the ESI†). Fig. 1 summarizes the characterization studies of Mn:CdS/ZnS QDs confirming the successful incorporation of Mn^{2+}. Fig. 1A shows the absorbance and photoluminescence (PL) spectra of the doped and undoped QDs. The doped and undoped QDs have nearly identical absorption spectra indicating similar nanocrystal size; however, their PL properties differ. The undoped QDs display excitonic emission at 488 nm compared with the doped QDs which exhibit PL at 581 nm. The new PL at 581 nm with a lifetime of 1.9 ms (Fig. S2†) corresponds to the $^4T_1 \rightarrow {}^6A_1$ transition of the Mn^{2+} dopant in a tetrahedral ligand field, which is lower in energy compared to the free-ion energy transition ($^4G \rightarrow {}^6S$) of Mn^{2+} due to the ligand field splitting of 3d orbitals into t_2 and e terms.[29] The quenching of the excitonic emission in doped QDs provides evidence of the incorporation of Mn^{2+} into the CdS lattice. The doping of Mn^{2+} in the QDs was further confirmed by electron paramagnetic resonance (EPR) spectroscopy (Fig. 1B). The presence of six strong lines corresponds to the hyperfine nuclear coupling to Mn^{2+} ($I = 5/2$), and the hyperfine splitting parameter A calculated from the EPR spectrum (65.1 × 10^{-4} cm^{-1}) is in line with Mn^{2+} in bulk CdS in a tetrahedral geometry.[30,31] In contrast, a surface Mn^{2+} ion has a much higher hyperfine splitting parameter.[32] Fig. 1C shows the powder X-ray diffraction (PXRD) spectrum of the doped QDs (black symbols) and the fit from Rietveld refinement (red line) indicating 45 wt% zinc blende and 55 wt% wurtzite phases.[33,34] The average QD size as imaged by TEM (Fig. 1D) is 5.6 ± 0.6 nm. The overall composition and size agree with those of the core/shell structure of the QDs, where the core Mn:CdS (wurtzite) is 4.5 nm in diameter based on excitonic absorption,[35] and the ZnS shell (zinc blende) is theoretically 0.7 nm in thickness (see the ESI†). The elongated structures observed in the TEM images were reported previously and suggested to result from the experimental conditions during shell growth. Stacking faults, specifically during the addition of the zinc precursor, lead to preferential elongation along the [002] direction.[36,37]

Photoreduction of viologens

We first investigated the photoreduction of methyl viologen (MV^{2+}) by the doped and undoped QDs. QD films on glass slides

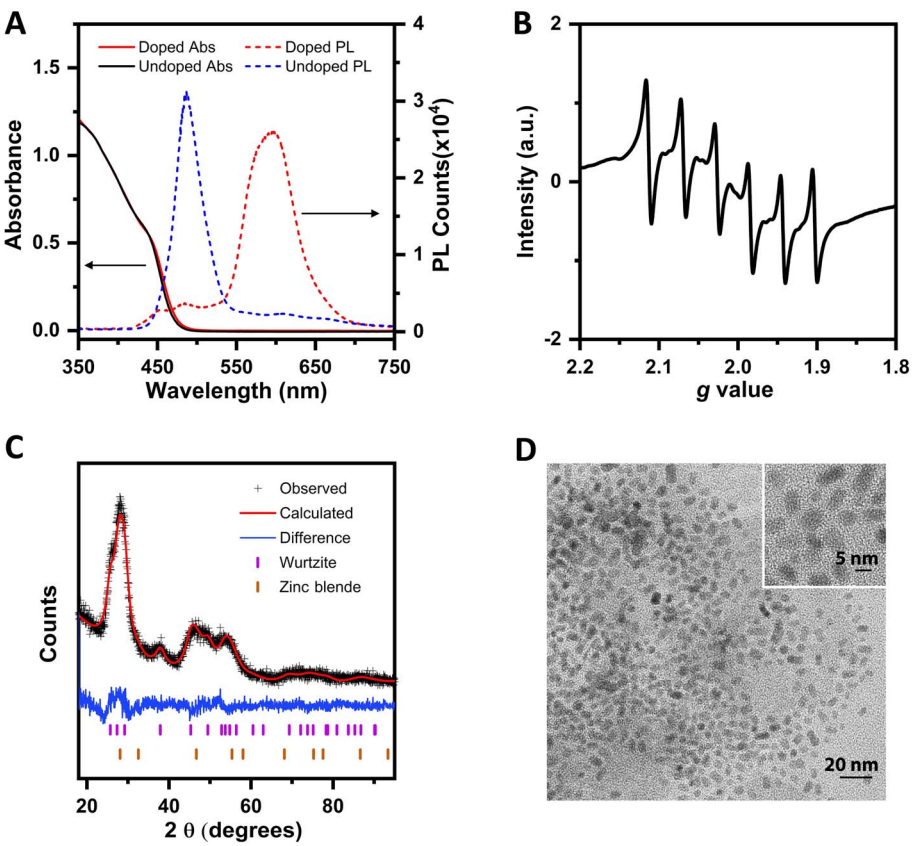

Fig. 1 Characterization studies of Mn^{2+}:CdS/ZnS QDs. (A) Absorbance (solid lines) and photoluminescence spectra (dashed lines) of doped Mn^{2+}:CdS/ZnS (red) and undoped CdS/ZnS (blue) QDs in toluene. (B) EPR spectrum of Mn^{2+}:CdS/ZnS with six lines resulting from energy splitting due to Mn^{2+} $I = 5/2$. (C) PXRD of doped QDs (experimental in black, calculated in red, and residual difference in blue). Phase analysis results in 55 wt% wurtzite and 45 wt% zinc blende. (D) TEM images of Mn^{2+}:CdS/ZnS QDs.

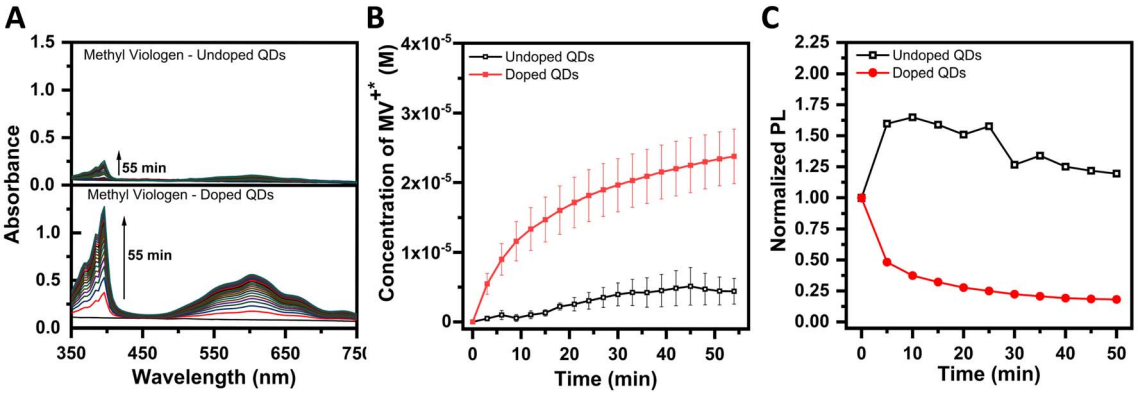

Fig. 2 Reduction of methyl viologen (MV^{2+}) to $MV^{+\bullet}$ by QDs. (A) UV-vis spectral evolution over time showing the formation of a charged radical ($MV^{+\bullet}$) in the presence of doped QDs (bottom) and undoped QDs (top) under 440 nm irradiation with methanol as a sacrificial electron donor. (B) Amount of $MV^{+\bullet}$ generated over the course of 55 min irradiation with doped (red) and undoped (black) QDs. Error bars are standard deviations. (C) Normalized photoluminescence (PL) intensity at 488 nm for the undoped QDs (black) and at 581 nm for the doped QDs (red) in the presence of MV^{2+} and methanol *vs.* irradiation time.

were placed in a 500 μM aqueous solution of methyl viologen. We determined the amount of QDs in the film by redispersing the uncross-linked QDs in toluene and measuring the solution absorbance. Methyl viologen is an electron acceptor and has a reduction potential of −0.446 V *vs.* NHE, which is below the conduction band energy of the QDs (see Fig. S3†). A single electron reduction of MV^{2+} leads to the singly charged radical $MV^{+\bullet}$, which absorbs at 396 and 605 nm. The appearance of the blue color in the viologen solution comes solely from the reduced species, contrary to a previous study that employed methylene blue,[38] where a decrease in the absorbance can arise from photoreduction as well as oxidative decomposition of the dye. Fig. 2A shows the evolution of absorption spectra of the viologen upon irradiation at 440 nm in the presence of doped *vs.* undoped QD films with MeOH as the sacrificial electron donor. The absorption of the viologen radical does not overlap with the incident irradiation at 440 nm and thus has no effect on the absorbance of QDs. In heterogeneous photocatalysis, the escape of charge carriers during the photoredox process deteriorates subsequent absorption and emission events; hence the presence of a sacrificial agent is crucial.[21,39] Fig. 2B summarizes the temporal concentration of $MV^{+\bullet}$ based on the absorbance and molar absorption coefficient at 396 nm for three trials. By considering the reaction as pseudo-first order, we obtained rate constants of 1.12×10^{-3} and 3.31×10^{-4} s^{-1} for doped and undoped QDs, respectively. This corresponds to a 3.4-fold enhancement in the rate of photoreduction of MV^{2+} by doped QDs *vs.* undoped QDs. We note that the excitation intensity we employed (85 mW cm^{-2}) was above the threshold at which the PL intensity of Mn^{2+} deviates from linear dependence on power (Fig. S4†). At this irradiation intensity, each QD was excited by 7400 photons per second, with 1 exciton produced per 0.36 ms (see the ESI†). Thus, Mn^{2+} states were saturated and Auger cross-relaxation was feasible.[15] We determined an internal quantum efficiency (IQE) of 2.9% for the doped QDs for the photoreduction of MV^{2+}. Additionally, we monitored the changes in the PL intensity of the doped and undoped QDs in the presence of MV^{2+}. Fig. 2C shows a small decay in the PL of the undoped QDs (after an initial increase due to photo-annealing), compared with an exponential-like decay (up to 75% attenuation) for the doped QDs. The significant bleach in the PL of the doped QDs in the presence of MV^{2+} corroborates the consumption of the photogenerated electrons and the efficient transfer of hot electrons from Mn:CdS/ZnS QDs. On the other hand, we observed a negligible decrease in the PL of the undoped QDs and only a small PL decay for the doped QDs without MV^{2+} in water (Fig. S5†). Doped QDs still exhibited a small PL decay in the absence of MV^{2+} because water is a weak electron acceptor and has been shown to be reduced to H_2 by the hot electrons of doped QDs.[24] The negligible change in the PL of the undoped dots with or without MV^{2+} indicates inefficient transfer of photoexcited electrons due to short exciton lifetimes even though energetically there is no barrier. Control experiments, including those in the absence of light or in the absence of QDs, showed no reaction of MV^{2+} (Fig. S6†). Besides the direct photoreduction of MV^{2+} by hot electrons in Mn:CdS/ZnS QDs, other reactive pathways involving MeOH are possible because oxidation of methanol by holes yields radicals ($^{\bullet}CH_2OH$ and $^{\bullet}CO_2^{-}$) and H_2,[40,41] which can also reduce MV^{2+}. The results nevertheless demonstrate the enhanced photoreduction capability of Mn:CdS/ZnS, in line with previous reports.[24]

Photoreduction of *meso*-1,2-dibromo-1,2-diphenylethane

Viologens are electron transfer agents with stable redox-active states and tunable nitrogen substituents. Various viologens, with octyl and heptyl substituents, undergo a change in solubility upon a single electron reduction and can act as electron shuttles between aqueous and nonaqueous phases.[42] Hence, we next explored a biphasic system incorporating heptyl viologen as the electron shuttle. The ability to separate the reactant from the photocatalyst, as in a biphasic system with a well characterised electron shuttle, can overcome the detrimental adsorption and accumulation of reactants on the reactive sites of the QDs. We show the versatility of the QD films in biphasic systems

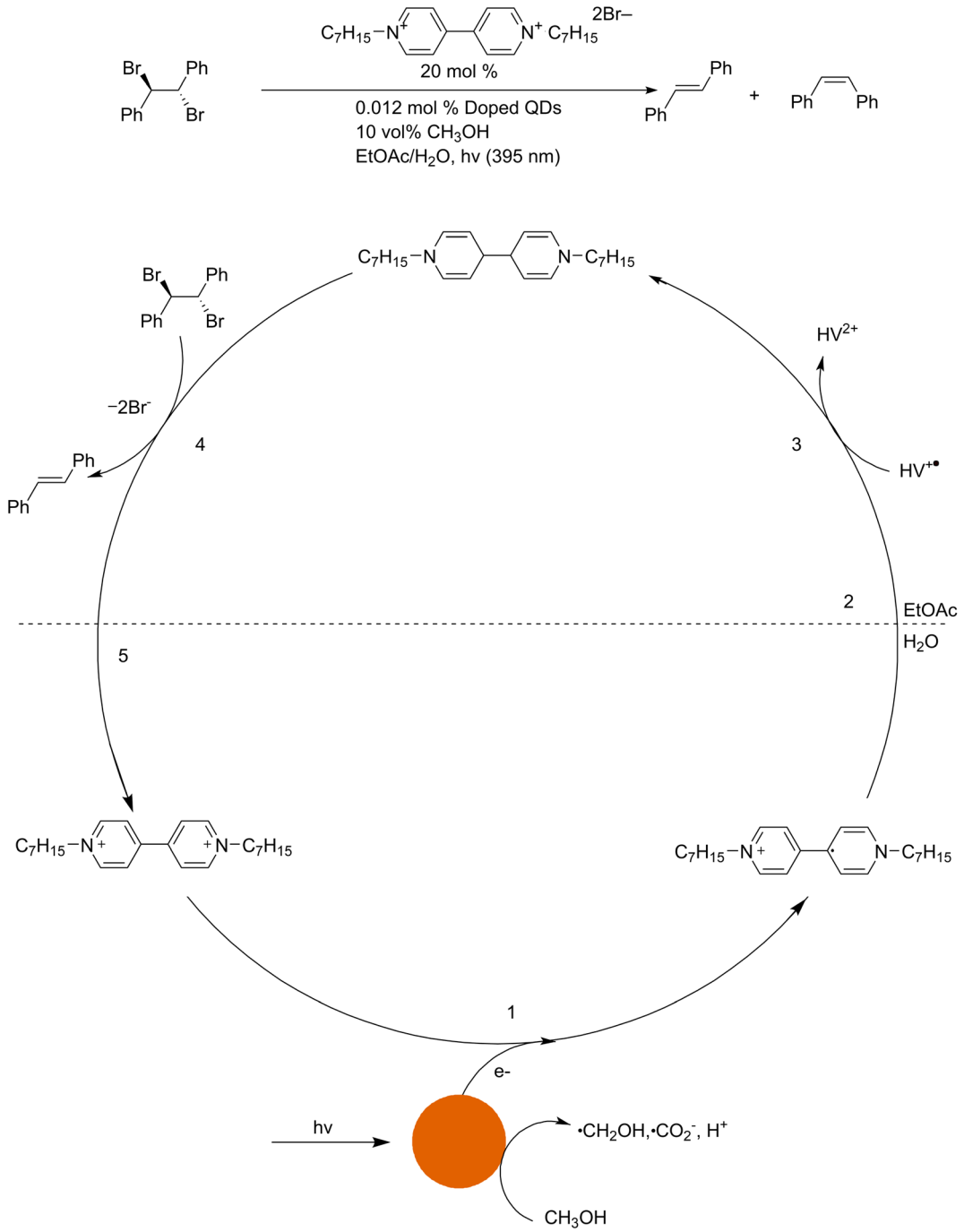

Scheme 2 Debromination of DDE with doped QDs as photocatalysts in a biphasic system (H_2O/EtOAc).

with the dehalogenation of *meso*-1,2-dibromo-1,2-diphenylethane (DDE). Scheme 2 shows the reaction mechanism for the dehalogenation reaction where the QDs replace the conventional Ru photocatalysts.[43–45] The catalytic cycle starts with the photoexcitation of QDs and the reduction of heptyl viologen (HV^{2+}) in the aqueous phase (step 1). Upon single electron reduction, the hydrophobicity of the heptyl viologen increases leading to its phase-transfer to the ethyl acetate layer (step 2). Disproportionation (step 3) then produces a doubly reduced viologen (HV^0) and HV^{2+} from two singly reduced charged radicals ($HV^{+\bullet}$). HV^0 eliminates the vicinal bromides in a two-electron reduction route forming *trans*-stilbene or *cis*-stilbene (step 4) and HV^{2+} is recycled back to the aqueous phase (step 5).

The biphasic dehalogenation reaction of DDE can be monitored *via* UV-vis spectroscopy. Fig. 3A shows the UV-vis spectra of the organic layer from a sample containing a doped QD film (in the aqueous phase) irradiated at 395 nm (150 mW cm^{-2}) for 24 h, with and without methanol (blue and red, respectively) *versus* that of a control in the dark (black). The vanishing peak

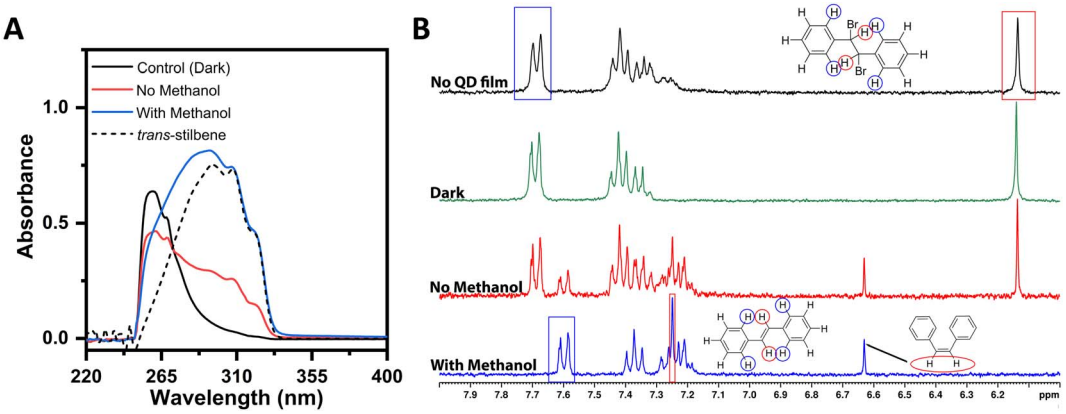

Fig. 3 (A) UV-vis spectra of the organic layer of the dehalogenation reaction of *meso*-1,2-dibromo-1,2-diphenylethane (DDE) in a biphasic system (H_2O/EtOAc), with heptyl viologen as an electron shuttle and methanol as a sacrificial agent under 395 nm irradiation, with (blue) and without methanol (red). The control reaction without irradiation is shown in black. The spectrum of pure *trans*-stilbene are illustrated with dashed lines. (B) ^{1}H NMR spectra for monitoring the reaction progress. An up-field shift in the doublets at 7.70–7.68 ppm to the doublets at 7.61–7.59 ppm shows the conversion of DDE to stilbene. NMR spectra of reactions 6, 3, 2 and 1 listed in Table 1 are shown as black, green, red, and blue trace in (B).

of the reactant at 260 nm and the evolution of a broad peak with a maximum at 294 nm indicate the formation of stilbene where the redshift of the product peak results from the expanded conjugation upon dehalogenation. The broad peak width, compared to the reference spectrum of pure *trans*-stilbene (dashed line) suggests the presence of the *cis*-isomer as well. *Trans* and *cis*-stilbene exhibit absorption peaks at 294 nm and 276 nm, respectively. To isolate the product for nuclear magnetic resonance (NMR) spectroscopy, the organic layer was simply separated, washed with water, and dried. Fig. 3B shows the ^{1}H NMR spectra of the samples obtained under various conditions. Control experiments (black and green curves corresponding to no QD film and in the dark, respectively) showed the signals of the starting material, including a singlet at 6.14 ppm. The doublet arising from the *ortho* hydrogens in the phenyl/aromatic rings of the reactant is at 7.68 ppm and shifts up-field to 7.59 ppm for the product stilbene. Signals from the *meta* and the *para*-protons in the aromatic rings of stilbene are in the range of 7.39–7.19 ppm, and the olefin protons show up as a singlet at 7.24 ppm and 6.63 ppm for the *trans*- and *cis*-isomers, respectively. Reactions catalyzed by the QDs showed ^{1}H NMR signals for both isomers. We monitored the conversion efficiency of the reaction *via* the integrated intensities of the doublets of the *ortho*-hydrogens (at 7.68 ppm for DDE and 7.59 ppm for stilbene). We achieved a conversion of 32% by the doped QDs without methanol, compared with a complete conversion of DDE to stilbene with 10 vol% of methanol. The progress of the reaction monitored by ^{1}H NMR is in line with the UV-vis observations and confirms that MeOH serves as an efficient sacrificial electron donor. Table 1 summarizes various reaction conditions and % of conversion photocatalyzed by doped or undoped QDs, where the conversion refers to the combined total of *trans*- and *cis*-stilbene. A control experiment without viologen (reaction 5) showed 0% conversion (Fig. S6†) and lowering the amount of HV^{2+} from 20 to 3 mol% (reaction 4, Fig. S7†) significantly reduced the yield, indicating the important role of HV in shuttling the electrons between the two phases. We observed variable isomeric ratios between replicate

Table 1 Summary of the dehalogenation reaction of DDE: biphasic system (H_2O/EtOAc) with HV^{2+} as an electron shuttle (reactions 1–6); monophasic reduction in EtOAc (without HV^{2+}, reactions 7–10). All reactions were irradiated for 24 h

Entry	DDE (μmol)	QDs	QDs (nmol)	QDs (mol%)	HV^{2+} (mol%)	Methanol (vol%)	% Conversion[a,b]
1	4	Doped	0.49	0.012	20	10	100
2	4	Doped	0.49	0.012	20	0	32
3 (dark)	4	Doped	0.49	0.012	20	10	0
4	4	Doped	0.49	0.012	3	10	17
5	4	Doped	0.49	0.012	0	10	0
6	4	None	0	0	20	10	0
7	4	Doped	0.49	0.012	0	10	100
8	4	Undoped	0.49	0.012	0	10	70
9	12	Doped	0.49	0.004	0	25	70
10	12	Undoped	0.49	0.004	0	25	45

[a] Includes *cis* and *trans* isomers. [b] % conversion determined by integrating doublets of products (7.61–7.59 ppm) and dividing by the sum of the areas of doublets of products and reactants (7.70–7.68 ppm).

runs, which may arise from rotational conformers[46] of the radical intermediate in the step-wise two-electron reduction mechanism as we did not detect photoisomerization of *trans*-stilbene under the irradiation condition or changes to the isolated product upon further irradiation. For the reaction photocatalyzed by doped QDs with 10% MeOH (reaction 1, at a scale of 1 mL of 4 mM DDE), we determined an approximate yield of 60% using the standard addition method by ^{1}H NMR spectroscopy.

The energy levels in Fig. S2† show that the LUMO of DDE is lower than the conduction band of CdS QD. Hence, the reaction can also be photocatalyzed directly by excited electrons of the QDs. Reactions 7–10 in Table 1 examined the conversion of DDE to stilbene in a single phase (*i.e.*, EtOAc with MeOH) without the electron shuttle. We tested different reaction conditions to compare the photocatalytic activity of doped *vs.* undoped QDs. An enhanced conversion was again observed for Mn:CdS/ZnS *vs.* CdS QDs, and 100% conversion was achieved with 0.012 mol% of doped QDs (based on ^{1}H NMR data, Fig. S8†). The results showed the consistent enhanced performance of the doped QDs *versus* their undoped counterparts, in aqueous and nonaqueous solvents, allowing for flexible reaction design and workups.

Reusability of Mn-doped QD films

Next, we investigated the reusability of the QD films by carrying out back-to-back reactions over 7 days, without any treatment. Fig. 4A shows that Mn:CdS/ZnS-coated vials yielded 100% conversion of DDE to stilbene in the first three runs (each 24 h); however, a decline in conversion to 84–55% was observed when the film was reused 4–7 times. We attribute the decrease in performance to several factors, including some detachment of the QDs from the walls of the vial and changes to the surface of the QDs due to the redox activities.[47] The latter has been noted in the literature, where surface ligands can detach or surface trap states related to photogenerated electrons and holes can

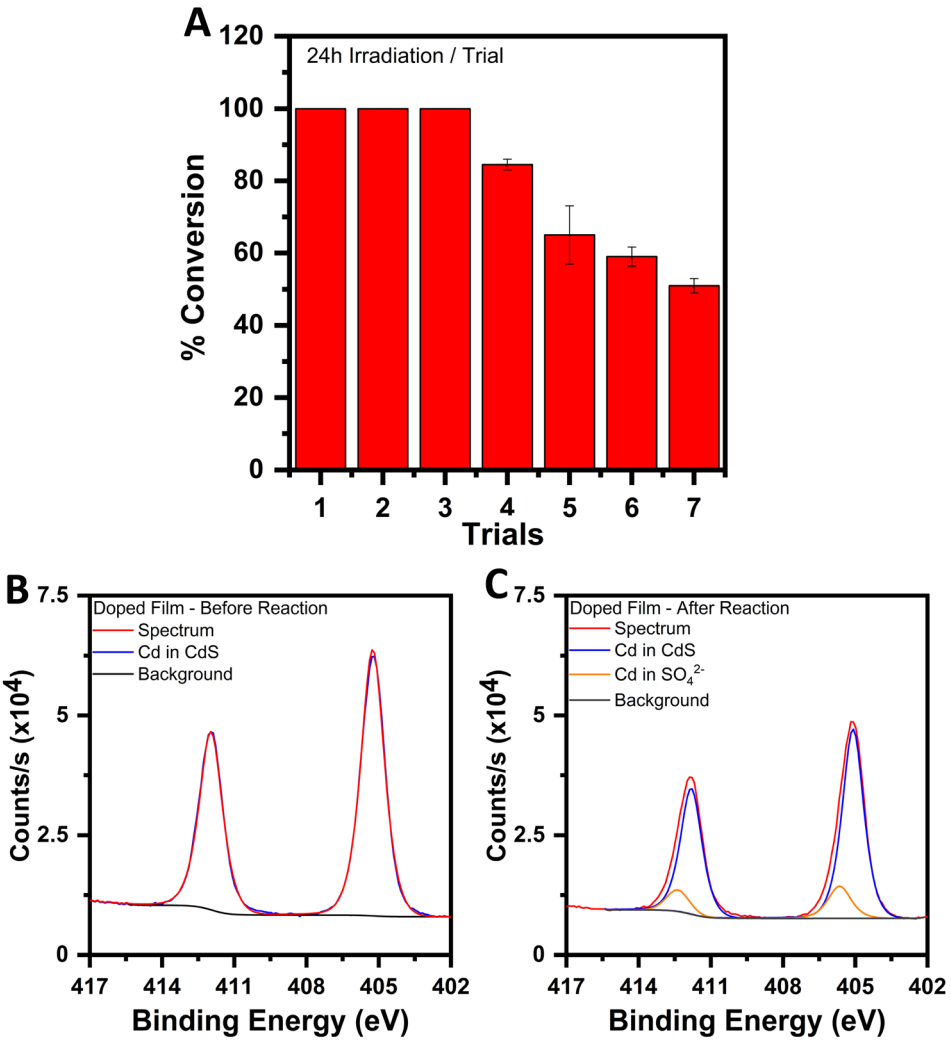

Fig. 4 (A) Percent conversion of DDE based on ^{1}H NMR data when coated vials were used back-to-back without any treatment. Each trial was 24 h of irradiation. Error bars are standard deviations of 3 replicates. (B) X-ray photoelectron spectra of Cd 3d in Mn:CdS/ZnS QD films before and (C) after the photoredox reaction of DDE. Experimental spectra are shown in red and fitted curves in other colors with each doublet corresponding to spin–orbit coupling of $3d_{5/2}$ and $3d_{3/2}$.

accumulate over time. The presence of trap states leads to non-radiative recombination of excitons and therefore negatively impacts the absorption, emission, and Auger processes.[48,49] We carried out X-ray photoelectron spectroscopy (XPS) on the films before and after the reaction to examine the changes to the QDs. Table S1† summarizes the findings of XPS. Initially, the binding energy (B.E.) of Cd 3d corresponded to only CdS (405.1 eV); however, an additional species, likely $CdSO_4$,[50] was detected at a B.E. of 405.4 eV after the dehalogenation reaction (Fig. 4B and C). The data are in line with the S 2p signal where the fraction of sulfate increased after the reaction (from 8.9% to 15.3%, Fig. S9†). Previous work reported that surface oxidation of the QDs leads to the conversion of sulfide to sulfate,[51] and sulfate ions can detach from the QDs over time and expose a fresh layer of the material susceptible to subsequent oxidation. Table S2† summarizes the atomic compositions of the samples before and after a catalytic run, which provide information on the quality of the QD films. Some detachment of QDs is evident by the increase in the In 3d signal (from the ITO substrate) after the reaction. It suggests a more exposed substrate, likely due to cracks or pin holes in the film after use. Therefore, additional passivation or repeated cross-linking of the QD films after a reaction trial may increase the durability of the QD films. Other sacrificial electron donors such as, S^{2-}/SO_3^{2-}, triethylamine, and EDTA, may be explored to increase the reusability of the QD films because they have higher redox potentials than methanol and may provide faster electron regeneration in the QD film. The ionic hole scavengers such as S^{2-}/SO_3^{2-} may be more compatible in aqueous media and yield more favourable kinetics.[40,52–54] We note that although microscopic changes on the QD surface were detected after 1 run, the decrease in reactivity was detected only after 3 runs (72 h of irradiation). Overall, the model reaction of stilbene production shows that doped QDs have superior photocatalytic activity compared with undoped QDs and may serve as replacements for transition metal complexes. Furthermore, the facile three-step film fabrication process to incorporate supported-QD catalysts in the reaction is desirable because ligand exchange of QDs to make them dispersible in reaction solvents is not needed and the reaction solution is readily separated from the QD film.

Photoreduction of nitrobenzene

Lastly, we applied the Mn:CdS/ZnS QD films to the photocatalytic reduction of nitrobenzene to aniline to investigate if the enhanced reduction from hot electrons of Mn-doped QDs is applicable broadly. The reduction of nitrobenzene to aniline is a six-electron and six-proton reaction that requires multiple electron transfer steps, *via* either the direct or indirect pathway.[55,56] Typical transition metal photocatalysts generate one exciton at a time; thus multielectron reductions need to be mediated *via* a cocatalyst or require additional intrinsic mechanisms that accumulate charge carriers.[57] Heterogeneous catalysts with large surface areas could circumvent these drawbacks. We carried out the photoreduction of nitrobenzene in 2-propanol with ammonium formate as the sacrificial electron donor and proton source, using reaction vials coated with the QDs. Fig. 5A and B show the UV absorption spectra of the reaction solutions over 30 min under irradiation at 395 nm as photocatalyzed by the doped QDs *vs.* undoped QDs. The absorbance peak of nitrobenzene is centered at 258 nm compared with those of aniline at 237 and 280 nm. The spectral changes in Fig. 5A and B suggest the reduction of nitrobenzene to aniline. We monitored the extent of the reaction from the absorbance peak of nitrobenzene at 258 nm, as summarized in Fig. 5C over three trials. We observed a rapid decrease (77%) in the nitrobenzene absorption within the first 10 min of the reaction photocatalyzed by the doped QDs. Conversely, the undoped QDs produced a slow linear decay of 26% during the first 10 min and the reaction remained incomplete up to 48 h of irradiation. For doped QDs, the ^{1}H NMR shows a complete conversion to aniline within 15 minutes (Fig. S10†). We obtained an internal quantum efficiency (IQE) of ~3% for the six-electron process to form aniline (see the ESI†) where 33 excitons were needed to reduce one nitrobenzene molecule to aniline. If all electron transfer steps are sequential[57] and similar in efficiency, the results suggest an impressive IQE of 55% for each step by the doped QDs.

The photoreduction of nitrobenzene at neutral pH serves as a direct investigation of the reducing power of the hot electrons from the Mn^{2+}-Auger relaxation process. Our reaction condition

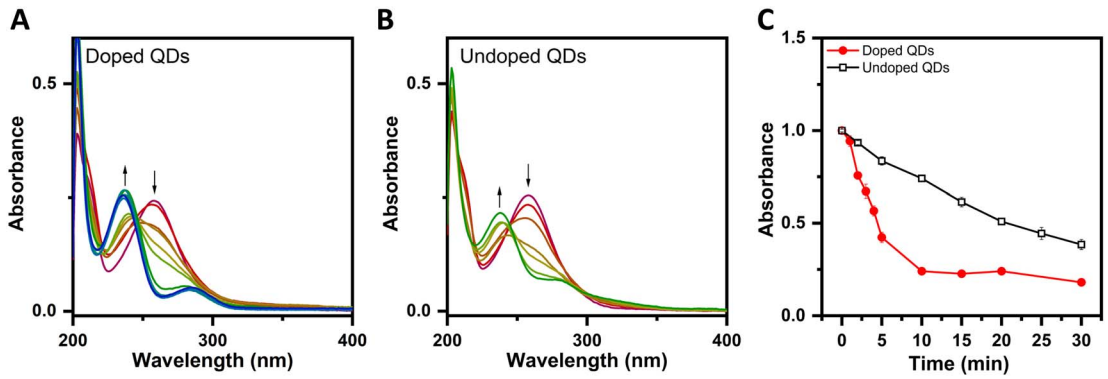

Fig. 5 Photoreduction of nitrobenzene (258 nm) to aniline (237 nm, 280 nm) monitored by UV-vis spectroscopy. (A) and (B) UV absorption spectra of the reaction solution photocatalyzed by doped (A) and undoped QDs (B) respectively. (C) Time dependence of absorbance of nitrobenzene at 258 nm for triplicate runs with doped (red) and undoped (black) QDs respectively. Error bars represent standard deviations.

at neutral pH is in contrast with that in previous work that employed undoped CdS QDs at an acidic pH,[57] where the reduction potential of nitrobenzene (−0.16 V *vs.* NHE at pH 4) was significantly below the energy of the CB of CdS. At neutral pH, the reduction potential of nitrobenzene is *ca.* −1.19 V *vs.* NHE, thus placing the LUMO of nitrobenzene close to the CB of QDs (see Fig. S3†). Photogenerated electrons at the band edge may therefore be insufficient in reducing power compared with hot electrons from Mn-doped QDs. However, the undoped QDs can drive this reaction at a moderate rate, suggesting non-negligible Auger relaxation in the undoped CdS that yields a small fraction of hot electrons. Notably, recent studies on Mn^{2+}-doped QDs showed that the rate of the Auger process outpaces that of intraband cooling,[16,17] and the exceptionally large uphill energy gain rates enabled by the spin-exchange Auger process lead to a large population of non-equilibrium hot electrons, which can undergo additional energy-transfer steps and upconversion to yield ejected electrons.[17] Other reaction pathways in our nitrobenzene reduction may involve H_2 generated by the oxidation of formate or 2-propanol by the photogenerated holes. Interestingly, a previous study showed that undoped QDs preferentially produced H_2 from formate while doped QDs generated more CO. Hence, the indirect reduction of nitrobenzene by H_2 may be more dominant in undoped QDs than in doped QDs. Taking together these differences, the significantly higher rate of photoreduction of nitrobenzene by the Mn:CdS/ZnS QDs highlights the strong reducing power of the Auger-mediated hot electrons.

Conclusions

The Mn^{2+}-doped QDs consistently showed increased photocatalysis of organic reactions compared with the undoped QDs, which we attribute to enhanced Auger processes in Mn:CdS/ZnS. The QD film coating shows high versatility in various solvents, can be employed in biphasic systems, is reusable, and reduces post-reaction purification needs. Improvements in the recyclability may be achieved by passivating the films between reaction intervals and further optimizing the sacrificial electron donors. Future directions include assembling the QD film on conductive substrates to yield a photoelectrochemical device, where secondary electrons can be injected to undergo Auger relaxation with the excited Mn^{2+} state, further boosting the hot-electron generation and opening new opportunities in photoelectrochemical-driven organic transformations. Overall, Mn-doped QDs show great promise as photocatalysts in organic reactions and may substantially increase the rate of photoreductions of challenging substrates recently demonstrated to be photocatalyzed by undoped CdS QDs.[58] Importantly, Auger cross-relaxation, which is otherwise a detrimental process in optoelectronic applications, presents a promising phenomenon in advancing QD-based photocatalysis.

Author contributions

B. M. carried out all experimental work and data analyses with the exception of XPS, which was performed by R. S. J. C. designed the project and provided supervision. B. M. and J. C. wrote the manuscript. All authors have given approval to the final version of the manuscript.

Conflicts of interest

The authors declare no competing conflict of interest.

Acknowledgements

Funding was supported by NSERC Discovery and Accelerator grants, and infrastructure support was from the Canada Foundation for Innovation. EPR data were acquired at Analest, Department of Chemistry at University of Toronto; TEM and XPS were performed at Ontario Centre for the Characterization of Advanced Materials, Department of Chemical Engineering and Applied Chemistry, University of Toronto. The authors thank Dr Gourevich, Dr Burns and Dr Hunter for technical assistance with TEM, EPR and NMR, respectively, and Prof. C. Caputo, Prof. T. Baumgartner, and Prof. A. Orellana for helpful discussions.

References

1 A. Pal, I. Ghosh, S. Sapra and B. König, *Chem. Mater.*, 2017, **29**, 5225–5231.
2 A. L. Efros, J. B. Delehanty, A. L. Huston, I. L. Medintz, M. Barbic and T. D. Harris, *Nat. Nanotechnol.*, 2018, **13**, 278–288.
3 A. J. Nozik, *Phys. E*, 2002, **14**, 115–120.
4 V. I. Klimov, *Los Alamos Sci.*, 2003, **28**, 214–220.
5 D. Y. Wang, Y. Y. Yin, C. W. Feng, Rukhsana and Y. M. Shen, *Catalysts*, 2021, **11**, 275.
6 J. A. Caputo, L. C. Frenette, N. Zhao, K. L. Sowers, T. D. Krauss and D. J. Weix, *J. Am. Chem. Soc.*, 2017, **139**, 4250–4253.
7 Y.-J. Yuan, D. Chen, Z.-T. Yu and Z.-G. Zou, *J. Mater. Chem. A*, 2018, **6**, 11606–11630.
8 D. A. Henckel, M. J. Enright, N. Panahpour Eslami, D. M. Kroupa, D. R. Gamelin and B. M. Cossairt, *Nano Lett.*, 2020, **20**, 2620–2624.
9 K. P. McClelland and E. A. Weiss, *ACS Appl. Energy Mater.*, 2019, **2**, 92–96.
10 M. J. Enright, K. Gilbert-Bass, H. Sarsito and B. M. Cossairt, *Chem. Mater.*, 2019, **31**, 2677–2682.
11 M. S. Kodaimati, K. P. McClelland, C. He, S. Lian, Y. Jiang, Z. Zhang and E. A. Weiss, *Inorg. Chem.*, 2018, **57**, 3659–3670.
12 J. H. Olshansky, T. X. Ding, Y. V. Lee, S. R. Leone and A. P. Alivisatos, *J. Am. Chem. Soc.*, 2015, **137**, 15567–15575.
13 S. C. Erwin, L. Zu, M. I. Haftel, A. L. Efros, T. A. Kennedy and D. J. Norris, *Nature*, 2005, **436**, 91–94.
14 C. J. Barrows, J. D. Rinehart, H. Nagaoka, D. W. deQuilettes, M. Salvador, J. I. L. Chen, D. S. Ginger and D. R. Gamelin, *J. Phys. Chem. Lett.*, 2017, **8**, 126–130.
15 L. R. Bradshaw, A. Hauser, E. J. McLaurin and D. R. Gamelin, *J. Phys. Chem. C*, 2012, **116**, 9300–9310.

16 R. Singh, W. Liu, J. Lim, I. Robel and V. I. Klimov, *Nat. Nanotechnol.*, 2019, **14**, 1035–1041.
17 C. Livache, W. D. Kim, H. Jin, O. V Kozlov, I. Fedin and V. I. Klimov, *Nat. Photonics*, 2022, **16**, 433–440.
18 Y. Dong, D. Rossi, D. Parobek and D. H. Son, *ChemPhysChem*, 2016, **17**, 660–664.
19 D. Parobek, T. Qiao and D. H. Son, *J. Chem. Phys.*, 2019, **151**, 120901.
20 X. B. Li, Z. K. Xin, S. G. Xia, X. Y. Gao, C. H. Tung and L. Z. Wu, *Chem. Soc. Rev.*, 2020, **49**, 9028–9056.
21 X. Yang and D. Wang, *ACS Appl. Energy Mater.*, 2018, **1**, 6657–6693.
22 U. Banin, N. Waiskopf, L. Hammarström, G. Boschloo, M. Freitag, E. M. J. Johansson, J. Sá, H. Tian, M. B. Johnston, L. M. Herz, R. L. Milot, M. G. Kanatzidis, W. Ke, I. Spanopoulos, K. L. Kohlstedt, G. C. Schatz, N. Lewis, T. Meyer, A. J. Nozik, M. C. Beard, F. Armstrong, C. F. Megarity, C. A. Schmuttenmaer, V. S. Batista and G. W. Brudvig, *Nanotechnology*, 2021, **32**, 42003.
23 W. Wu, G. Liu, Q. Xie, S. Liang, H. Zheng, R. Yuan, W. Su and L. Wu, *Green Chem.*, 2012, **14**, 1705–1709.
24 Y. Dong, J. Choi, H. K. Jeong and D. H. Son, *J. Am. Chem. Soc.*, 2015, **137**, 5549–5554.
25 D. Parobek, J. R. Meeder, J. Puthenpurayil, M. Nippe and D. H. Son, *J. Mater. Chem. A*, 2020, **8**, 12984–12989.
26 M. A. White, A. L. Weaver, R. Beaulac and D. R. Gamelin, *ACS Nano*, 2011, **5**, 4158–4168.
27 D. Yu, B. L. Wehrenberg, P. Jha, J. Ma and P. Guyot-Sionnest, *J. Appl. Phys.*, 2006, **99**, 104315.
28 X. Peng, M. C. Schlamp, A. V Kadavanich and A. P. Alivisatos, *J. Am. Chem. Soc.*, 1997, **119**, 7019–7029.
29 R. Beaulac, P. I. Archer, S. T. Ochsenbein and D. R. Gamelin, *Adv. Funct. Mater.*, 2008, **18**, 3873–3891.
30 A. M. Schimpf, S. T. Ochsenbein and D. R. Gamelin, *J. Phys. Chem. Lett.*, 2015, **6**, 457–463.
31 A. K. Koh and D. J. Miller, *Solid State Commun.*, 1986, **60**, 217–222.
32 T. A. Kennedy, E. R. Glaser, P. B. Klein and R. N. Bhargava, *Phys. Rev. B: Condens. Matter Mater. Phys.*, 1995, **52**, R14356–R14359.
33 H. M. Rietveld, *J. Appl. Crystallogr.*, 1969, **2**, 65–71.
34 B. H. Toby, *Powder Diffr.*, 2006, **21**, 67–70.
35 L. E. Brus, *J. Chem. Phys.*, 1984, **80**, 4403–4409.
36 F. V. Mikulec, M. Kuno, M. Bennati, D. A. Hall, R. G. Griffin and M. G. Bawendi, *J. Am. Chem. Soc.*, 2000, **122**, 2532–2540.
37 B. O. Dabbousi, J. Rodriguez-Viejo, F. V. Mikulec, J. R. Heine, H. Mattoussi, R. Ober, K. F. Jensen and M. G. Bawendi, *J. Phys. Chem. B*, 1997, **101**, 9463–9475.
38 H. Y. Chen, T. Y. Chen, E. Berdugo, Y. Park, K. Lovering and D. H. Son, *J. Phys. Chem. C*, 2011, **115**, 11407–11412.
39 X. Qiu, Y. Zhang, Y. Zhu, C. Long, L. Su, S. Liu and Z. Tang, *Adv. Mater.*, 2021, **33**, 2001731.
40 F. Costantino and P. V. Kamat, *ACS Energy Lett.*, 2022, **7**, 242–246.
41 A. S. Hainer, J. S. Hodgins, V. Sandre, M. Vallieres, A. E. Lanterna and J. C. Scaiano, *ACS Energy Lett.*, 2018, **3**, 542–545.
42 L. Striepe and T. Baumgartner, *Chem.–Eur. J.*, 2017, **23**, 16924–16940.
43 R. Maidan, Z. Goren, J. Y. Becker and I. Willner, *J. Am. Chem. Soc.*, 1984, **106**, 6217–6222.
44 I. Willner, Z. Goren, D. Mandler, R. Maidan and Y. Degani, *J. Photochem.*, 1985, **28**, 215–228.
45 J. Twilton, C. C. Le, P. Zhang, M. H. Shaw, R. W. Evans and D. W. C. MacMillan, *Nat. Rev. Chem.*, 2017, **1**, 0052.
46 P. Fawell, J. Avraamides and G. Hefter, *Aust. J. Chem.*, 1990, **43**, 1421–1430.
47 J. Tang, K. W. Kemp, S. Hoogland, K. S. Jeong, H. Liu, L. Levina, M. Furukawa, X. Wang, R. Debnath, D. Cha, K. W. Chou, A. Fischer, A. Amassian, J. B. Asbury and E. H. Sargent, *Nat. Mater.*, 2011, **10**, 765–771.
48 E. N. Bodunov and A. L. Simões Gamboa, *J. Phys. Chem. C*, 2019, **123**, 25515–25523.
49 W. W. Yu, L. Qu, W. Guo and X. Peng, *Chem. Mater.*, 2003, **15**, 2854–2860.
50 D. Meissner, C. Benndorf and R. Memming, *Appl. Surf. Sci.*, 1987, **27**, 423–436.
51 A. P. Alivisatos, *J. Phys. Chem.*, 1996, **100**, 13226–13239.
52 F. Zhao, Q. Li, K. Han and T. Lian, *J. Phys. Chem. C*, 2018, **122**, 17136–17142.
53 J. R. Herance, B. Ferrer, J. L. Bourdelande, J. Marquet and H. Garcia, *Chem.–Eur. J.*, 2006, **12**, 3890–3895.
54 J. Schneider, A. Vaneski, G. R. Pesch, A. S. Susha, W. Y. Teoh and A. L. Rogach, *APL Mater.*, 2014, **2**, 126102.
55 A. Mahata, R. K. Rai, I. Choudhuri, S. K. Singh and B. Pathak, *Phys. Chem. Chem. Phys.*, 2014, **16**, 26365–26374.
56 E. A. Gelder, S. D. Jackson and C. M. Lok, *Chem. Commun.*, 2005, 522–524.
57 S. C. Jensen, S. B. Homan and E. A. Weiss, *J. Am. Chem. Soc.*, 2016, **138**, 1591–1600.
58 J. K. Widness, D. G. Enny, K. S. McFarlane-Connelly, M. T. Miedenbauer, T. D. Krauss and D. J. Weix, *J. Am. Chem. Soc.*, 2022, **144**, 12229–12246.

